

High-performance frequency stabilization of ultraviolet diode lasers by using dichroic atomic vapor spectroscopy and transfer cavity

Danna Shen(申丹娜), Liangyu Ding(丁亮宇), Qiuxin Zhang(张球新), Chenhao Zhu(朱晨昊), Yuxin Wang(王玉欣), Wei Zhang(张威), Xiang Zhang(张翔)

Citation: Chin. Phys. B . 2020, 29(7): 074210 . **doi:** 10.1088/1674-1056/ab8c41
Journal homepage: http://cpb.iphy.ac.cn; http://iopscience.iop.org/cpb

What follows is a list of articles you may be interested in

Vertical profile of aerosol extinction based on the measurement of O_4 of multi-elevation angles with MAX-DOAS

Fusheng Mou(牟福生), Jing Luo(雒静), Suwen Li(李素文), Wei Shan(单巍), Lisha Hu(胡丽莎)

Chin. Phys. B . 2019, 28(8): 084212 . **doi:** 10.1088/1674-1056/28/8/084212

Phase-dependent double optomechanically induced transparency in a hybrid optomechanical cavity system with coherently mechanical driving

Shi-Chao Wu(吴士超), Li-Guo Qin(秦立国), Jian Lu(鹿建), Zhong-Yang Wang(王中阳)

Chin. Phys. B . 2019, 28(7): 074204 . **doi:** 10.1088/1674-1056/28/7/074204

Anisotropic stimulated emission cross-section measurement in Nd: YVO_4

Rui Guo(郭瑞), Yijie Shen(申艺杰), Yuan Meng(孟鸢), Mali Gong(巩马理)

Chin. Phys. B . 2019, 28(4): 044204 . **doi:** 10.1088/1674-1056/28/4/044204

Active hyperspectral imaging with a supercontinuum laser source in the dark

Zhongyuan Guo(郭中源), Yu Liu(刘煜), Xin Zheng(郑鑫), Ke Yin(殷科)

Chin. Phys. B . 2019, 28(3): 034206 . **doi:** 10.1088/1674-1056/28/3/034206

Modulation transfer spectroscopy based on acousto-optic modulator with zero frequency shift

Chen-Fei Wu(吴晨菲), Xue-Shu Yan(颜学术), Li-Xun Wei(卫立勋), Pei Ma(马沛), Jian-Hui Tu(涂建辉), Jian-Wei Zhang(张建伟), Li-Jun Wang(王力军)

Chin. Phys. B . 2018, 27(11): 114203 . **doi:** 10.1088/1674-1056/27/11/114203

High-performance frequency stabilization of ultraviolet diode lasers by using dichroic atomic vapor spectroscopy and transfer cavity*

Danna Shen(申丹娜)[1], Liangyu Ding(丁亮宇)[1], Qiuxin Zhang(张球新)[1], Chenhao Zhu(朱晨昊)[1], Yuxin Wang(王玉欣)[1], Wei Zhang(张威)[1,2], and Xiang Zhang(张翔)[1,2,†]

[1] *Department of Physics, Renmin University of China, Beijing* 100872, *China*

[2] *Beijing Key Laboratory of Opto-electronic Functional Materials and Micro-nano Devices, Renmin University of China, Beijing* 100872, *China*

(Received 10 March 2020; revised manuscript received 16 April 2020; accepted manuscript online 23 April 2020)

We develop a high-performance ultraviolet (UV) frequency stabilization technique implemented directly on UV diode lasers by combining the dichroic atomic vapor laser lock and the resonant transfer cavity lock. As an example, we demonstrate a stable locking with measured frequency standard deviations of approximately 200 kHz and 300 kHz for 399 nm and 370 nm diode lasers in 20 min. We achieve a long-term frequency drift of no more than 1 MHz for the target 370 nm laser within an hour, which is further verified with fluorescence count rates of a single trapped $^{171}Yb^{+}$ ion. We also find strong linear correlations between lock points and environmental factors such as temperature and atmospheric pressure. Our approach provides a simple and stable solution at a relatively low cost, and features flexible control, high feedback bandwidth and minimal power consumption of the target UV laser.

Keywords: frequency stabilization, ultraviolet diode laser, dichroic atomic vapor spectroscopy, transfer cavity

PACS: 42.55.–f, 42.60.–v, 42.60.Lh, 32.30.–r **DOI:** 10.1088/1674-1056/ab8c41

1. Introduction

Ultraviolet (UV) lasers are increasingly used in numerous photonics applications in research and industry, including quantum information processing, atomic frequency standards, photoemission spectroscopy, and laser photolithography. Some applications have very stringent requirements for central frequencies of lasers, e.g., the experiments related to cold atoms or trapped ions.[1–3] Recently, several conventional UV laser diodes and their counterpart external cavity grating feedback diode lasers (ECDLs) have become widely available. They are more compact and lightweight, more energy-efficient, require less maintenance, and cost much lower than traditional frequency-doubling UV lasers. However, since UV-coated optical devices are relatively inefficient and easily damaged, the frequency stabilization for UV diode lasers is usually more difficult than traditional UV lasers, for which the frequency stabilization can actually appear in the visible or near-infrared (NIR) spectral region by using excess longer wavelength lasers.

In general, a laser frequency stabilization system should at least consist of an absolute frequency reference and a frequency locking component. Commonly used absolute frequency references include absorption lines, other stable lasers and Fabry-Pérot (FP) cavities, especially high-finesse cavities made of ultra-low thermal expansion (ULE) materials and installed in specially designed stable vacuum housings. The corresponding frequency locking schemes include the saturation absorption dither locking (SADL),[4–9] polarization spectroscopy (PS),[10–13] the modulation transfer spectroscopy (MTS),[14–19] the dichroic atomic vapor laser lock (DAVLL),[20–22] the Pound–Drever–Hall (PDH) technique,[23] the scanning transfer cavity lock (STCL),[24–27] the offset sideband lock,[28,29] the injection and phase locked loop lock, etc.[30] However, the widely used rich absorption lines of Rb or iodine,[31] as well as the frequency-shifting fiber electro-optic modulator (EOM) with a wide tuning range, are generally unavailable in the UV spectral region. It is also usually difficult to coat a transfer FP cavity in the operating wavelength range from UV to NIR. Therefore, for UV diode lasers with relatively limited output power, the best practice should be a UV absorption line scheme, but this will only apply if the target lock point is fortunately located near a strong absorption line.

In order to overcome these limitations, we develop a high-performance frequency stabilization technique that combines the DAVLL and the resonant transfer cavity lock. The new approach needs an auxiliary UV laser with less strict central frequency requirement. We first lock the auxiliary laser to a strong absorption spectral line using the DAVLL method, then the frequency lock is passed to the target UV laser through the resonant transfer cavity. The lock point of the target UV laser can be fine tuned by adjusting the lock point of the DAVLL in a huge real-time frequency tuning range up to GHz, which can cover the whole free spectral range (FSR) of conventional

*Project supported by the National Natural Science Foundation of China (Grant Nos. 11704408 and 91836106), the Beijing Natural Science Foundation, China (Grant No. Z180013), and the Joint Fund of the Ministry of Education, China (Grant No. 6141A020333xx).

†Corresponding author. E-mail: siang.zhang@ruc.edu.cn

© 2020 Chinese Physical Society and IOP Publishing Ltd

FP cavities. All frequency locking and shifting functions, including automatic lock-point finding and automatic two-way top-of-fringe transfer lock, are implemented by digital signal processing algorithms[32,33] based on field-programmable gate array (FPGA) technology. We build and test this approach in a trapped ion experiment. The main apparatus is a Yb hollow-cathode lamp (HCL) for the DAVLL and a conventional FP cavity for the resonant transfer cavity lock. By analyzing and cancelling laser power and polarization jittering, we achieve frequency standard deviations of 202 kHz and 309 kHz for the auxiliary 399 nm laser and the target 370 nm laser, respectively. Furthermore, we analyze the relationship between lock points and environmental parameters, e.g., temperature and atmospheric pressure, and find strong linear correlations that can be reasonably explained. Finally, we achieve a long-term frequency drift of no more than 1 MHz for the 370 nm laser and verify it by recording and analyzing fluorescence counts rate of a single trapped $^{171}Yb^{+}$ ion.

2. Experimental setup

The entire experimental system is placed in a closed box as schematically shown in Fig. 1. The 399 nm laser beam enters the box through a polarization-maintaining fiber (SM-300), and is then divided into two beams by a half-wave plate (HWP) and a polarized-beam splitter (PBS), which are used for the DAVLL and the transfer cavity, respectively. The 399 nm beam for the DAVLL passes a Glan–Taylor prism (PGT5010) with a high extinction ratio to ensure that the output beam is purely linear polarized, and then hits the center of the Yb HCL. A pair of permanent magnet rings are placed close to the HCL to generate a stable magnetic field, which causes a relatively large Zeeman splitting for the atoms in the HCL. Left-handed and right-handed circularly polarized beams pass through a quarter-wave plate (QWP) and become vertically or horizontally polarized. The two polarized beams are then separated by a Wollaston prism (WP10), and measured by photodetectors (DET100). We install narrow-linewidth optical filters and short-focus lens with adjustable distance in front of each photodetector, which significantly improves the signal-to-noise ratio of PD signals by reducing the interference of background light and increasing the beam intensity shining on the PD. The other 399 nm beam for the transfer cavity is combined with a weak (< 10 μW) 370 nm laser beam through a dichroic mirror. The double pass AOM path is used for frequency shifting of testing purpose and can be optional. The combined beam enters a commercial confocal FP cavity (model SA200-3B) through a lens for pattern matching. The transmitted 370 nm and 399 nm beams are separated again by a dichroic mirror and measured with PDs.

The analog voltage signals of PDs are converted to digital signals through an eight-channel 16-bit analog-to-digital converter (ADC, AD7606). These signals undergo a series of digital signal processing, then convert into feedback voltages by two two-channel 16-bit digital-to-analog converters (DAC, DAC8563), and finally output to the piezoelectric

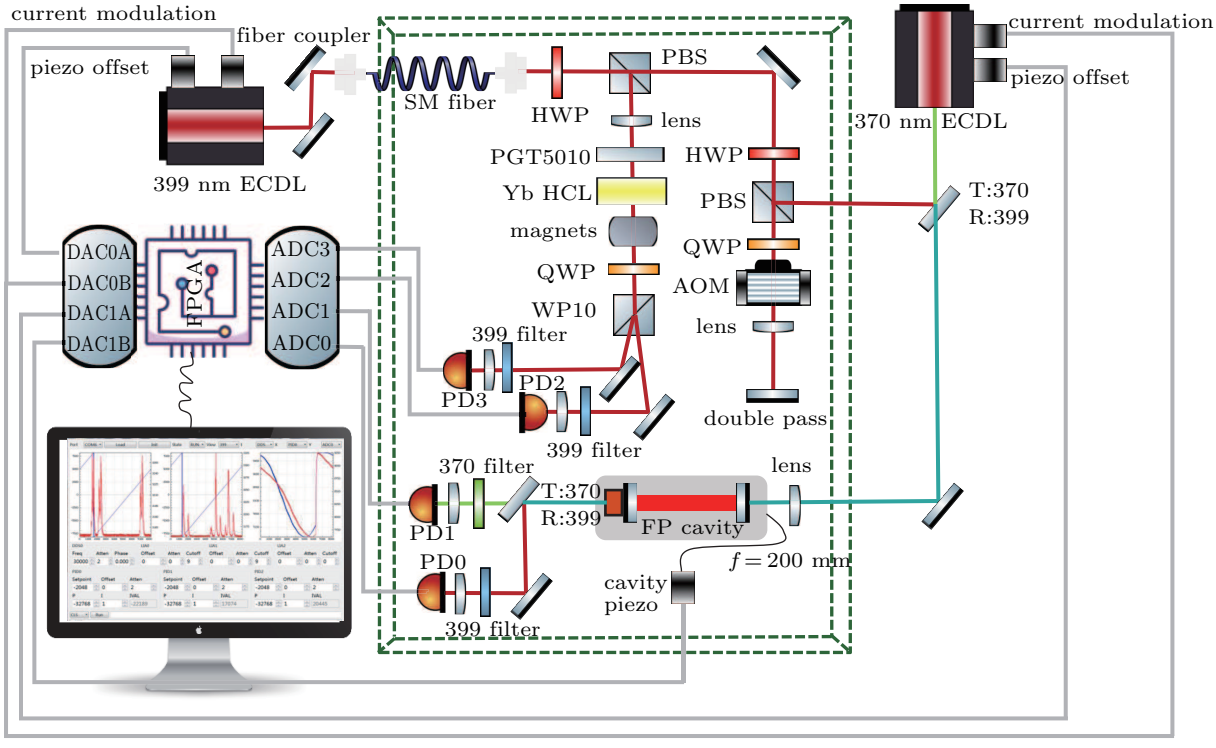


Fig. 1. Experimental setup. AOM, acousto-optic modulator; ECDL, external cavity dioder laser; HCL, hollow-cathode lamp; HWP; half-wave plate; PBS, polarization splitting prism; PD, photodetector; PGT5010, Glan–Taylor prism; QWP, quarter-wave plate; WP10, Wollaston prism.

ceramics of the laser or the FP cavity to implement the stabilization of frequency or cavity length. Digital signal processing algorithms including digital signal synthesizers, digital lock-in amplifiers, digital low-pass filters, and digital proportional-integral-derivative (PID) controllers, are implemented through FPGA (Spartan 6 XC6SLX9, 100 MHz clock) programming on a low-cost Mojo V3 development board. All the hardware modules, including the transfer function generator for testing purpose, are wrapped into standard trigger-driven input/output interfaces. All the logical connections can be reconfigured on the fly from our PC program, which can also communicate with the FPGA and automatically find the lock point. We only need to adjust some parameters on the computer via a user-friendly interface and confirm the position of the lock point to complete the entire frequency stabilization process. The overall feedback bandwidth is around 100 kHz mainly limited by the maximum sampling speed of the ADC.

This all-digital design greatly simplifies the topology of connection wires, reduces the impact of noise during signal processing and improves robustness. The algorithms and parameters can be simulated, tested and tuned with standard FPGA simulation technology. As we will explain later, it enables us to replace the traditional expensive balanced photodetector with a pair of UV-optimized single detectors, which have higher quantum efficiencies and eliminate common mode laser amplitude noise. Except for the commercial FP cavity, the total cost of our solution is less than 1000 dollars and does not require any special modulation functionality of the laser.

3. Dichroic atomic vapor spectroscopy

The DAVLL method subtracts the absorption signals of Zeeman level transitions as the frequency discriminator error signal, and consumes much less laser power than other pump-based spectroscopy methods. We choose a low-cost HCL (model Yb HL-1) with an operating voltage of approximately 132 V and an operating current of approximately 5 mA. We use its absorption line near 398.9 nm as the absolute frequency reference. Using HCL instead of evacuated heat pipe or vacuum chamber makes the apparatus much simpler, and potentially enables self-test for the target 370 nm laser since the HCL has both atoms and ions inside. The single beam nature of the DAVLL method also allows us to use conventional cylindrical HCLs instead of expensive opto-galvanic models.

As shown in Fig. 2(a), the excited state $^1\mathrm{P}_1$ of the Yb atom contains three degenerate Zeeman energy levels with energies

$$\Delta E(^1\mathrm{P}_1)/\hbar = (14.5\ \mathrm{MHz/mT})mB \quad (\text{for } m = \pm 1). \tag{1}$$

A high precision wavelength meter (model WS8) is used to measure optical frequencies and estimate frequency stabilities. It is based on calibrated interferometers and has a resolution of 200 kHz. We first measure the absorption spectrum obtained from PD2 by scanning the piezo voltage offset of the 399 nm laser. For magnets at different positions, the wavelength of the central $m = 0$ absorption valley is always stable at 398.91134 nm. We adjust the position of magnets and wave plates until all three absorption valleys of Zeeman transitions can be identified clearly, as shown in Fig. 2(b). The magnetic field intensity produced by permanent magnets at the center of the HCL is approximately 76 mT (measured without HCL). This corresponds to a frequency gap of approximately 1.1 GHz, which is in consistence with the measured wavelength difference between $m = 0$ and $m = -1$ transitions. The 200 MHz additional frequency gap between $m = 1$ and $m = 0$ transitions is believed to be caused by isotope shifts. However, we notice that it is difficult to observe clear absorption spectrum of both circular polarizations simultaneously, which may also explain an abnormal half frequency splitting as mentioned in Ref. [21]. In this work, we choose to use absorption signals of $m = 0$ and $m = -1$, and scan the piezo voltage offset of the 399 nm laser at the central wavelength 398.91154 nm. The top panel of Fig. 2(c) shows the signal of V_{ADC2} and V_{ADC3}, which are respectively absorption signals of the π and σ^- polarization beams obtained from PD2 and PD3. The error signal V_{ADC23} is obtained by directly subtracting the two signals, as shown in the bottom panel of Fig. 2(c). The slope of this error signal is 265 MHz/V, which is obtained by linear fitting the center portion. Thus with our ± 10 V 16-bit ADC, the minimum detectable laser frequency change in the DAVLL setup is 81 kHz, which is already better than our wavelength meter, and can be further enhanced by preamplifiers to achieve the best performance.

However, this original error signal of the DAVLL method may be affected by beam power, polarization and optical path jitter. Therefore, we use polarization-maintaining fibers instead of free space to conduct the laser beam to the HCL in the closed box, and use $(V_{\mathrm{ADC2}} - V_{\mathrm{ADC3}})/(V_{\mathrm{ADC2}} + V_{\mathrm{ADC3}} - V_0)$ instead of $V_{\mathrm{ADC2}} - V_{\mathrm{ADC3}}$ as the error signal to eliminate the jitter of optical power, where V_0 is the sum of the PDs' dark voltages. This normalized error signal is processed by the PID controller and converted to voltage by the DAC, and then fed back to the piezoelectric ceramics of the 399 nm laser to compensate fluctuations in laser frequency.

With this setup, the measured frequency jitter of the locked 399 nm laser is limited within 1 MHz (-0.7 MHz to 0.3 MHz) in 20 min, and the standard deviation is 202 kHz, which is close to the instantaneous linewidth of the diode laser, as shown in the left panel of Fig. 3. Over a longer period of time, a linear correlation between frequency drift and temperature change inside the box is observed, as shown in the right panel of Fig. 3. The temperature coefficient of the lock point change obtained by linear fitting is 8.458 MHz/K, which indi-

cates a twice coefficient of 16.9 MHz/K for the σ^- polarization absorbtion or 1.16 mT/K for the magnetic field intensity in the HCL. Based on this observation, we install a temperature heating controller in the box and keep the temperature around 302 K with 0.1 K precision. Since the relative temperature coefficient of permanent magnets' remanence is negative and is at most -0.05 %/K, we believe that the dominant reason for this 1.6 %/K temperature coefficient should be the distance between the permanent magnets and the HCL mainly due to thermal expansion and contraction.

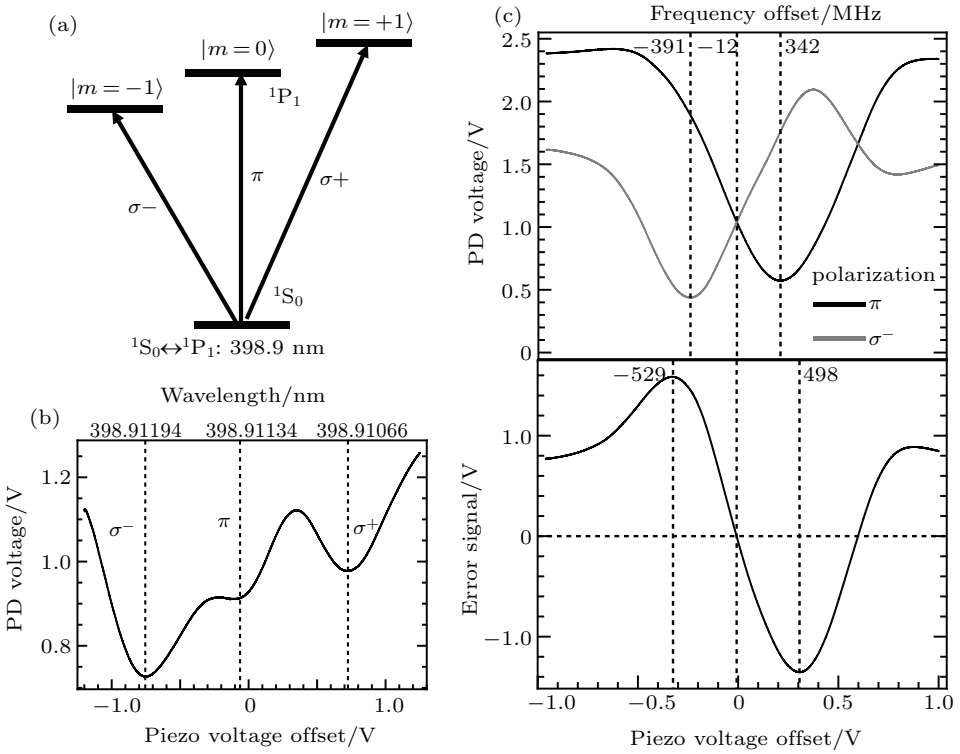


Fig. 2. (a) The level structure of Zeeman levels within the excited manifold $^1P_1$ of the Yb atom. (b) The Zeeman level absorption valleys (black dashed) corresponding to the three transitions shown in (a) can be well identified in the absorption spectrum. (c) The absorption spectrum of the π (top, black solid) and σ^- (top, gray solid) polarization, and the error signal (bottom, black solid).

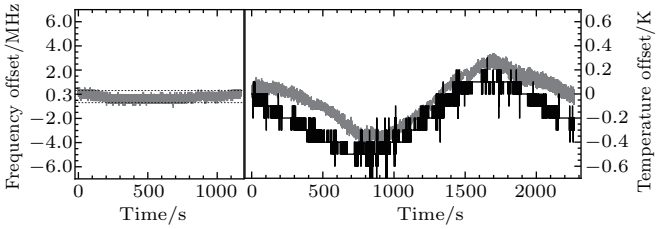


Fig. 3. Relative frequency offsets of the 399 nm laser (gray) for (left) a short-term within 20 min and (right) a long-term within 40 min measurement as well as relative temperature offsets in the box (black).

4. Transfer cavity

The resonant transfer cavity lock scheme is implemented by first locking the FP cavity length to the stabilized 399 nm laser and then locking the 370 nm laser to the FP cavity length. For both the cases we use the simple top-of-fringe method instead of the PDH method and obtain the derivative of the transmitted peak signal by modulating the phase of the laser. The slope-shape demodulated differential signal holds an approximate linear dependence on the incident laser frequency or the cavity length over the entire peak range, hence can be used as the error signal, as shown in Fig. 4. By locking at the zero point of derivative, the resonant transfer cavity lock effectively avoids possible non-linearity and noise of timing or electronic levels, and has a much higher sensitivity and feedback bandwidth than the common used scanning transfer cavity lock. The fineness of the commercial FP cavity we use is above 200, which is sufficient to suppress short-term frequency jitter to a reasonable range.

After the frequency stabilization of the 399 nm laser is achieved, we first scan the length of the FP cavity to a frequency scanning range equal to the FSR of 1.5 GHz, and find a single transmitted peak signal. A current modulation of 5 kHz and 0.05 mA is applied to the 399 nm laser, and the demodulated slope-shape error signal is fed back to the length of the FP cavity through a PID controller. After the cavity length is stabilized, we scan the piezo voltage offset of the 370 nm laser to find its transmitted peak that resonates with the cavity length. The same current modulation is also applied to the 370 nm laser and the demodulated slope-shape error signal is fed back to the piezo voltage offset of the 370 nm laser through another PID controller. By adjusting the lock point wavelength of the 399 nm laser to 398.911691 nm, the 370 nm laser is transfer locked at 369.526275 nm, which is the optimal Doppler cooling frequency for our trapped $^{171}Yb^+$ ion setup.

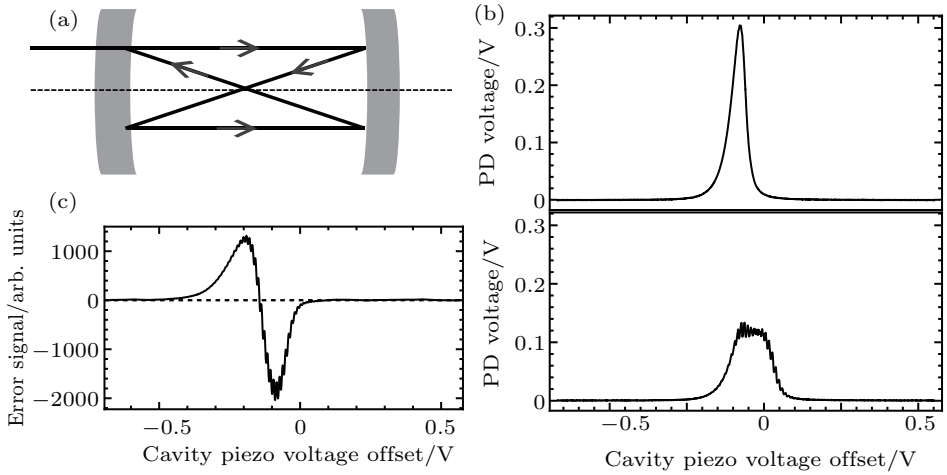


Fig. 4. (a) Diagram of the confocal FP cavity. (b) The transmitted peak signal without (top) and with (bottom) modulating the phase of the laser when scanning the cavity length. (c) The demodulated error signal when scanning the cavity length.

The performance of the transfer cavity is characterized by monitoring frequency ratio between the 399 nm and 370 nm lasers. The frequency ratio is very stable for a time period less than 10 min, as shown in the left panel of Fig. 5, indicating that the transfer relationship is trustworthy. Over a longer period of time, a linear correlation between the drift of the frequency ratio and the atmospheric pressure inside the box is observed, which is caused by different refractive indices changes between the 399 nm and 370 nm lasers, as shown in the right panel of Fig. 5. The linear coefficient is fitted to be 2.05×10^{-8} kPa^{-1}, or -2.39×10^{-8} kPa^{-1} for reverse frequency ratio, which corresponds to -18 MHz/kPa frequency drift for the 370 nm laser assuming the 399 nm laser is stable. To minimize induced fluctuations, we try to keep both the laboratory door and the box airtight, and obtain a relatively stable atmospheric pressure between 101.76 kPa and 101.79 kPa.

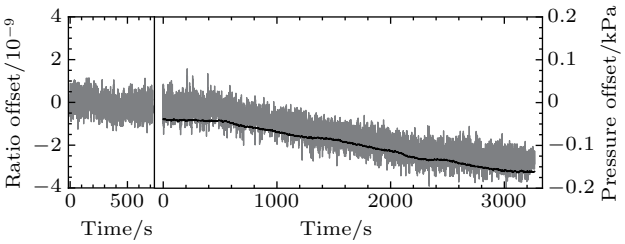


Fig. 5. Relative offsets of frequency ratio between the 399 nm and 370 nm lasers (gray) during (left) a short-term and (right) a long-term measurement as well as relative offsets of the atmospheric pressure in the box (black).

With stabilized temperature and atmospheric pressure, we can finally stabilize the target 370 nm laser in a relatively long time scale. In Fig. 6, we show the frequency drifting of the 370 nm laser under different conditions: laser is not locked, locked with a wavelength meter, and locked using our method. The measured frequency standard deviations are 8.768 MHz, 685 kHz and 309 kHz, respectively. Under both locked conditions, the feedback stabilization eliminates the frequency drift generally encountered by lasers in free-running mode. The maximum deviations remain within a window of less than ± 2 MHz for the wavelength meter lock, and ± 1 MHz for our method. Although the wavelength meter is very accurate and expensive, the milliseconds exposure time and channel switching time, as well as the software-based PID regulator, limit its feedback bandwidth to only a few Hz, making its performance inferior to our method. The result of our method is further confirmed by monitoring fluorescence count rates of a single trapped $^{171}Yb^{+}$ ion, as shown in the right panel. Since most fluorescence count rates are between 20.8 kHz and 23.2 kHz, the long-term frequency drift of the 370 nm laser must be in the ± 1 MHz range (-25.8 MHz to -23.8 MHz) according to the measured fluorescence spectrum shown in the inset, which is appropriate for efficient laser cooling and state detection on the 19.7 MHz S–P transition in $^{171}Yb^{+}$.

The slope of the fluorescence count rates with respect to detuning frequency around the lock point, 1.2 kHz/MHz, can also be used to convert the fluctuation of the fluorescence count rates into the 370 nm laser frequency fluctuation. A rough estimation of the frequency stability of the frequency-stabilized 370 nm laser is made by this calibration. The true stability, however, should be obtained from a beat frequency measurement between two identical systems. To characterize the time domain behavior of our frequency-stabilized 370 nm laser, we collect a 3-hour data and calculate the Allan deviation $\sigma_y(\tau)$ of the frequency fluctuation either measured by the wavelength meter or calibrated from the fluorescence count rates as a function of the average time τ, as shown in Fig. 7. The frequency stability calibrated from the fluorescence count rates decreases from 239 kHz at $\tau = 1$ s and reaches an almost minimum value of 46 kHz at $\tau = 1000$ s. The frequency stability measured by the wavelength meter first decreases from 149 kHz at $\tau = 1$ s but finally goes up to 261 kHz at $\tau = 1000$ s. This different behavior may indicate a long term drift of the wavelength meter itself.

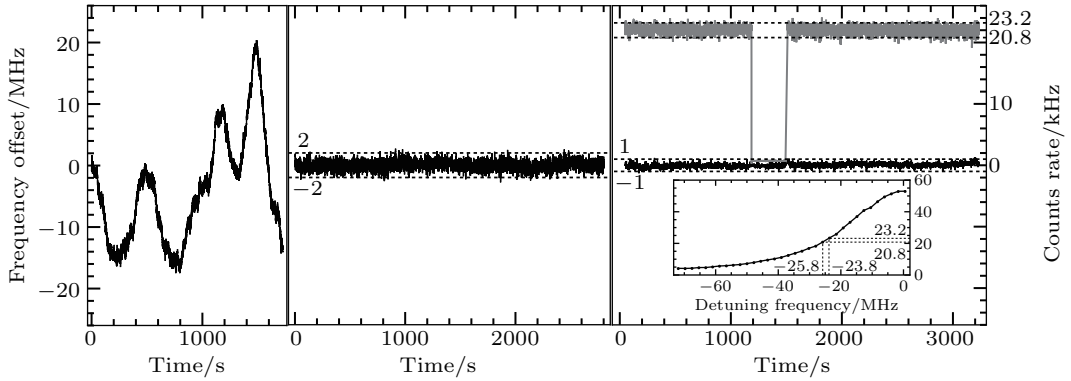


Fig. 6. The left, middle and right panels show the frequency drifting (black) when the laser is not locked, locked with a wavelength meter, and locked using our method, respectively. The right panel shows a stable ion fluorescence counts rate (gray) and the inset shows the fluorescence spectrum with respect to detunning frequency in MHz. The "jump" of ion fluorescence counts rate indicates an occasional ion "dark" event.

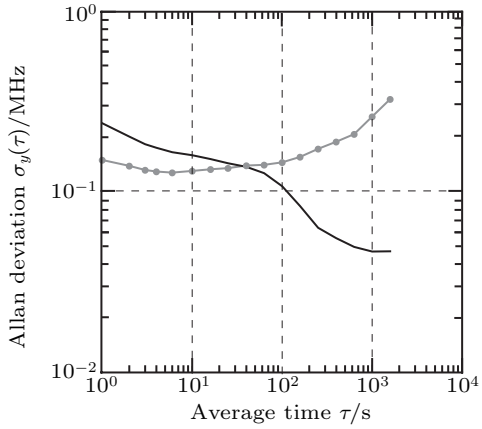


Fig. 7. Allan deviation $\sigma_y(\tau)$ of the frequency fluctuation either measured by the wavelength meter (gray) or calibrated from the fluorescence count rates (black) as a function of average time τ.

5. Conclusions

In summary, we have demonstrated a high-performance laser frequency stabilization technique implemented directly on UV diode lasers, by combining the dichroic atomic vapor laser lock and the resonant transfer cavity lock. The target UV laser can be locked tightly at any central frequency by adjusting the lock point of the auxiliary laser in a GHz huge real-time frequency tuning range. Our approach provides a simple and stable solution at a relatively low cost, and features flexible control, high feedback bandwidth and minimal power consumption of the target UV laser.

Although this is a general technique, it is particularly suitable for trapped ion quantum experiments, in which the cooling laser is the target UV laser and the ionization laser is the auxiliary laser. In these experiments, the cooling laser usually has shorter wavelengths, lower available power, and is divided into several parts for state initialization and state detection as well with different modulations. The ionization laser usually has longer wavelength, higher available power, and becomes idle once ions are loaded. Therefore, a fraction of its power can be shared and its frequency can be adjusted to assist the stabilization of the cooling laser at the ion manipulation stage. In fact, since we use the spectroscopy of the same atomic species as the trapped ions, the lock point of the ionization laser is close to the optimal ionization frequency near the atomic resonance. Due to the broadening of laser power and atomic beam velocity distribution, we have successfully reloaded and cooled ions during experiments without unlocking. By selecting hollow-cathode lamps with corresponding element materials, our method can be extended to trapped ion experiments with other elements such as Ca and Ba, and will be more widely used with the improvement of ultraviolet laser diode technology.

The short-term stability of our method can be further improved by replacing the laser current modulation with an EOM. To improve the long-term stability of the transfer lock, the FP cavity can be placed in a vacuum housing with temperature control. If the required lock point of the auxiliary laser for the transfer lock is fortunately near the atomic resonance, or if there is a resonant UV EOM with a design frequency close to the required frequency shift, the tuning range requirement can be much lower. Then the DAVLL method can be replaced with the SADL or MTS method by locking at the Zeeman levels. By using a solenoid to adjust the strength of the magnetic field, the Zeeman lock point can be continuously adjusted in the range of hundreds of MHz.[16] In this way, we will eliminate potential long-term drift caused by laser power and polarization fluctuations, thereby obtaining a more clearly defined absolute reference frequency.

Acknowledgment

The authors thank M. L. Cai and Q. X. Mei for helpful discussions.

References

[1] Zhang X, Zhang K, Shen Y C, Zhang S N, Zhang J N, Yung M H, Casanova J, Pedernales J S, Lamata L, Solano E and Kim K 2018 *Nat. Commun.* **9** 1

[2] Guan H, Huang Y, Liu P L, Bian W, Shao H and Gao K L 2015 *Chin. Phys. B* **24** 054213

[3] Heinzen D J and Wineland D J 1990 *Phys. Rev. A* **42** 2977

[4] Wan J H, Liu C and Wang Y H 2016 *Chin. Phys. B* **25** 044204

[5] Zhang X, Huang K K, Xu H, Xu Z X, Li N and Lu X H 2012 *Chin. Phys. Lett.* **29** 074206
[6] Zhou T, Qi X H, Wang Q, Xiong W, Duan Jun, Zhou X J and Chen X Z 2010 *Chin. Opt. Lett.* **8** 496
[7] Dammalapati U, Norris I and Riis E 2009 *J. Phys. B: At. Mol. Opt. Phys.* **42** 165001
[8] Zhang Z, Wang X L and Lin Q 2009 *Opt. Express* **17** 10372
[9] Haroche S and Hartmann F 1972 *Phys. Rev. A* **6** 1280
[10] Zhu S B, Chen T, Li X L and Wang Y Z 2014 *J. Opt. Soc. Am. B* **31** 2302
[11] Lee M W, Jarratt M C, Marciniak C and Biercuk M J 2014 *Opt. Express* **22** 7210
[12] Sun J F, Yin S Q, Xu Z, Hong T and Wang Y Z 2013 *Chin. Phys. B* **22** 024207
[13] Do H D, Moon G and Noh H R 2008 *Phys. Rev. A* **77** 032513
[14] Ru N, Wang Y, Ma H J, Hu D, Zhang L and Fan S C 2018 *Chin. Phys. B* **27** 074201
[15] Wu C F, Yan X S, Wei L X, Ma P, Tu J H, Zhang J W and Wang L J 2018 *Chin. Phys. B* **27** 114203
[16] Cheng B, Wang Z Y, Wu B, Xu A P, Wang Q Y, Xu Y F and Lin Q 2014 *Chin. Phys. B* **23** 104222
[17] Wang W L, Ye J, Jiang H L, Bi Z Y, Ma L S and Xu X Y 2011 *Chin. Phys. B* **20** 013201
[18] Noh H R, Park S E, Li L Z, Park J D and Cho C H 2011 *Opt. Express* **19** 23444
[19] McCarron D J, King S A and Cornish S L 2008 *Meas. Sci. Technol.* **19** 105601
[20] Zhang L J, Zhang H, Zhao Y T, Xiao L T and Jia S T 2019 *Chin. Phys. B* **28** 084211
[21] Kim J I, Park C Y, Yeom J Y, Kim E B and Yoon T H 2003 *Opt. Lett.* **28** 245
[22] Corwin K L, Lu Z T, Hand C F, Epstein R J and Wieman C E 1998 *Appl. Opt.* **37** 3295
[23] Wang H M, Xu Z S, Ma S C, Cai M H, You S H and Liu H P 2019 *Opt. Lett.* **44** 5816
[24] Subhankar S, Restelli A, Wang Y, Rolston S L and Porto J V 2019 *Rev. Sci. Instrum.* **90** 043115
[25] Jackson S, Sawaoka H, Bhatt N, Potnis S and Vutha A C 2018 *Rev. Sci. Instrum.* **89** 033109
[26] Uetake S, Matsubara K, Ito H, Hayasaka K and Hosokawa M 2009 *Appl. Phys. B* **97** 413
[27] Bohlouli Z P, Afrousheh K and Martin J D D 2006 *Rev. Sci. Instrum.* **77** 093105
[28] Milani G, Rauf B, Barbieri P, Bregolin F, Pizzocaro M, Thoumany P, Levi F and Calonico D 2017 *Opt. Lett.* **42** 1970
[29] Yang B D, Wang J, Liu H F, He J and Wang J M 2014 *Opt. Commun.* **319** 174
[30] Jiao Y C, Li J K, Wang L M, Zhang H, Zhang L J, Zhao J M and Jia S T 2016 *Chin. Phys. B* **25** 053201
[31] Eloranta E W and Razenkov I A 2006 *Opt. Lett.* **31** 598
[32] Jørgensen N B, Birkmose D, Trelborg K, Wacker L, Winter N, Hilliard A J, Bason M G and Arlt J J 2016 *Rev. Sci. Instrum.* **87** 073106
[33] Feng G S, Wu J Z, Wang X F, Zheng N X, Li Y Q, Ma J, X L T and Jia S T 2015 *Chin. Phys. B* **24** 104211